Active Flutter Control Using Generalized Unsteady Aerodynamic Theory

John W. Edwards*
NASA Dryden Flight Research Center, Edwards, Calif.
and
John V. Breakwell† and Arthur E. Bryson Jr.†
Stanford University, Stanford, Calif.

This paper describes the application of generalized unsteady aerodynamic theory to the problem of active flutter control. The controllability of flutter modes is investigated. It is shown that the response of aeroelastic systems is composed of a portion due to a rational transform and a portion due to a nonrational transform. The oscillatory response characteristic of flutter is due to the rational portion, and a theorem is given concerning the construction of a linear, finite-dimensional model of this portion of the system. The resulting rational model is unique and does not require state augmentation. Active flutter control designs using optimal regulator synthesis are presented.

Nomenclature

A,B = weighting matrices [Eq. (17)]
A_i = matrix of residues at ith pole
$A(s)$ = $n \times n$ system matrix
a = location of elastic axis
a_∞ = speed of sound
B_a,B_{nc},B_s = $n \times n$ damping coefficient matrices
b = section semichord
C = $m \times N$ feedback gain matrix
$C(\bar{s})$ = generalized Theodorsen function
c = distance from origin to trailing-edge control surface hingeline
c_{l_α} = section lift-curve slope
d = distance from origin to leading-edge control surface hingeline
diag = diagonal matrix
E^n = Euclidean n space
F = $N \times N$ stability matrix
G = $n \times m$ ($N \times m$) control distribution matrix
g = structural damping
H = $p \times N$ output matrix
$H(s)$ = $p \times m$ transfer function matrix
h = plunge coordinate
I = identity matrix
i = $\sqrt{-1}$
i,j,k,r = dummy variables
J = performance index
K_a,K_{nc},K_s = $n \times n$ stiffness coefficient matrices
$k_{(\cdot)}$ = spring constant
L = $n \times 1$ aerodynamic load vector
M = Mach number
M_a,M_{nc},M_s = $n \times n$ inertia coefficient matrices
$M^{(\cdot)}$ = moment associated with dot coordinate, positive tail down for α and β, nose down for γ
m = dimension of u
m_s = section mass per unit length
N = dimension of X
$N_{(\cdot)}$ = numerator zeros associated with $(\cdot)$ transfer function
n = number of degrees of freedom of section
P = lift force on section, positive downward
p = dimension of y
$Q(s)$ = $n \times n$ matrix of aerodynamic load coefficients
R,S_1,S_2 = matrices [Eq. (5)]
res = residue
$r_{(\cdot)}$ = radius of gyration associated with $(\cdot)$ coordinate
s = $\sigma + i\omega$ Laplace transform variable
s_i = eigenvalue
T = transformation matrix
t = time
U = airspeed
u = $m \times 1$ input vector
X = $N \times 1$ state vector
$X(s)$ = Laplace transform of $x(t)$
x = coordinate along section chord
$x_{(\cdot)}$ = static unbalance associated with $(\cdot)$ coordinate
$x,x(t)$ = $n \times 1$ modal coordinate vector
y = $p \times 1$ output vector
z = coordinate perpendicular to chord
z_a = downwash
α = pitch coordinate
β = trailing-edge flap coordinate
γ = leading-edge flap coordinate
$\zeta_{(\cdot)}$ = viscous damping coefficient associated with $(\cdot)$ coordinate
Λ = $N \times N$ diagonal stability matrix
μ = section mass ratio
ρ = atmospheric density
Φ = Laplace transform of φ
φ = velocity potential
$\omega_{(\cdot)}$ = natural frequency associated with $(\cdot)$ coordinate

Subscripts

c = command
j = jth element of a vector
$i\cdot,\cdot i$ = ith row and ith column of a matrix

Superscripts

T = matrix transpose
$\bar{(\ )}$ = a variable nondimensionalized by b/U

Received July 18, 1977; presented as Paper 77-1061 at the AIAA Guidance and Control Conference, Hollywood, Fla., Aug. 8-10, 1977 (in bound volume of Conference papers); revision received Sept. 6, 1977.

Index categories: Aeroelasticity and Hydroelasticity; Guidance and Control.

*Aerospace Engineer. Member AIAA.
†Professor, Department of Aeronautics and Astronautics. Member AIAA.

Introduction

FLUTTER is an unstable motion caused by an interaction between structural vibrations and the aerodynamic forces which results in the extraction of energy from the airstream. Traditional methods of flutter analysis have proceeded by 1) determining the vibration modes of the structure with no aerodynamic forces present; 2) calculating the aerodynamic forces on the wing due to simple harmonic oscillations of the in vacuo normal modes as functions of Mach number, altitude, and reduced frequency; and 3) searching for combinations of these parameters for which simple harmonic motion yields an equilibrium between the structural inertial forces and the unsteady aerodynamic forces. Such combinations describe the flutter boundary.

One reason for the assumption of simple harmonic oscillations has been the belief that unsteady aerodynamic theory was valid only for such motions. This is a severe restriction for the control engineer trying to synthesize active flutter control logic. Nevertheless, active flutter control laws have been formulated using these techniques.[1-4]

Edwards[5,6] and Edwards et al.[7] have shown that the restriction of unsteady aerodynamic theory to simple harmonic oscillations is unnecessary. This paper applies their generalized unsteady aerodynamic theory to the problem of active flutter control techniques. The generalized aerodynamic theory is summarized, and examples of the calculation of exact solutions are given. The use of augmented state approximate solutions also is summarized. The construction of a model of the rational portion capable of describing flutter phenomena is stated as a theorem, and the model is used to study active flutter control. In addition, the controllability of flutter modes by aerodynamic control surfaces is investigated, and flutter mode controllability is used to study the aerodynamic energy flutter suppression technique.

Generalized Unsteady Aerodynamics

Three-dimensional flexible wings may be described by partial differential equations with nonhomogeneous forcing terms derived from the unsteady pressure distribution on the wing. The pressure distribution may be found by solving the linearized unsteady aerodynamic partial differential equation. Since this paper is concerned with unsteady aerodynamic effects, the complexity of the partial differential equation of the structure is unnecessary, and the simpler model of a two-dimensional typical section is considered.

The typical section that is analyzed is shown in Fig. 1. It has leading- and trailing-edge control surfaces that are unbalanced aerodynamically (hinge lines at the leading and trailing edge), which simplifies the description of the aerodynamics. Linear and torsional springs (k_h and k_α) act at the section elastic axis to restrain motion in the plunge h and pitch α degrees of freedom, and torsional restraining springs (k_β and k_γ) act at the control surface hinge lines. All linear coordinates (x, z, h) are nondimensionalized by the semichord b. The equations of motion are derived by following the conventions described in Refs. 8-10 which result

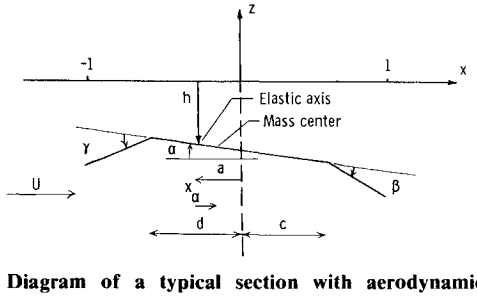

Fig. 1 Diagram of a typical section with aerodynamically unbalanced leading- and trailing-edge control surfaces.

in the following equation:

$$M_s\ddot{x} = -K_s x - B_s\dot{x} + (1/m_s b^2)L + Gu \tag{1}$$

where the subscript s indicates that the matrix operators are of structural origin and

$$x^T = [h\ \alpha\ \beta\ \gamma]$$

$$L^T = [Pb\ M^\alpha\ M^\beta\ M^\gamma]$$

$$u^T = [\beta_c\ \gamma_c]$$

The matrices M_s, K_s, B_s, and G are as follows:

$$M_s = \begin{bmatrix} 1 & x_\alpha & x_\beta & x_\gamma \\ x_\alpha & r_\alpha^2 & [r_\beta^2 + x_\beta(c-a)] & [x_\gamma(d-a) - r_\gamma^2] \\ x_\beta & [r_\beta^2 + x_\beta(c-a)] & r_\beta^2 & 0 \\ x_\gamma & [x_\gamma(d-a) - r_\gamma^2] & 0 & r_\gamma^2 \end{bmatrix}$$

$$K_s = \text{diag}\ [\omega_h^2\ r_\alpha^2\omega_\alpha^2\ r_\beta^2\omega_\beta^2\ r_\gamma^2\omega_\gamma^2]$$

$$B_s = \text{diag}\ [0\ 0\ 2\zeta_\beta\omega_\beta r_\beta^2\ \ 2\zeta_\gamma\omega_\gamma r_\gamma^2]$$

$$G = \begin{bmatrix} 0 & 0 \\ 0 & 0 \\ r_\beta^2\omega_\beta^2 & 0 \\ 0 & r_\gamma^2\omega_\gamma^2 \end{bmatrix}$$

Equation (1) describes a four-degree-of-freedom model. Two- and three-degree-of-freedom models may be obtained from Eq. (1) by deleting the appropriate rows and columns of the matrices and vectors.

The aerodynamic load vector L is derived from solutions of the linearized partial differential equation of unsteady aerodymamics:

$$\nabla^2\varphi - \frac{1}{a_\infty^2}\frac{\partial^2\varphi}{\partial t^2} - \frac{2M}{a_\infty}\frac{\partial^2\varphi}{\partial x\partial t} - M^2\frac{\partial^2\varphi}{\partial x^2} = 0 \tag{2}$$

with the boundary condition of tangential flow at the airfoil surface:

$$\frac{\partial\varphi}{\partial x}(x,0,t) = \frac{\partial z_a}{\partial t} + U\frac{\partial z_a}{\partial x} \tag{3}$$

where $z_a(x,t) = -h - \alpha x$. For subsonic flow, a unique solution of Eq. (2) is obtained by using the Kutta condition of smooth flow off the trailing edge.

Traditional solutions of Eq. (2) assume the existence of a separable solution; furthermore, they assume simple harmonic motion. These assumptions were based on the belief that the solutions were not valid for stable airfoil motions.[11,12] The loads L required to perform stability analyses are derived from appropriate partial derivatives of φ. The requirement of simple harmonic solutions and the complexity of the numerical calculations led to the introduction of artificial structural damping g.[13] This artifice facilitated the calculation of flutter boundaries and provided some information regarding subcritical flutter conditions. However, the commonly used structural damping model is unphysical,[5] and predictions based upon g values become suspect as the value of g increases. Thus, traditional U-g flutter analysis is not very satisfactory as a synthesis technique for active flutter control.

References 5-7 show that the restriction of the aerodynamic theory to simple harmonic motions is unnecessary and that traditional unsteady aerodynamic theory may be generalized to arbitrary values of the complex frequency s, where $s=\sigma+i\omega$. Edwards[5] shows that the Laplace transformation of Eqs. (2) and (3) leads to a solution $\Phi(x,z,s) = \Phi_I(x,z,s) + \Phi_2(x,z,s)$. The Φ_I solution is formally identical to the traditional solution of the unsteady aerodynamic problem with $i\omega$ generalized to s, whereas the Φ_2 solution is linear in the initial conditions of the motion of the wing. It was argued[5-7] that the resulting generalized loads were of the form $Q_I(s)X(s)+Q_2(s)x(0)$ and that only the Φ_I solution was required to determine stability. However, this conclusion is open to question, as shown by the following example.

For two-dimensional, subsonic flow, the inverse Laplace transformation of the Φ_I solution has been calculated for the case of an airfoil plunging impulsively at Mach 0.8. Figure 2 compares this transient loading to that calculated by Ref. 14, which is exact for $Ut/b \leq 8.0$. Further calculations of the pressure distributions along the chord during the starting transient show that the pressure differences in the figure for $Ut/b \leq 8.0$ are due to traveling pressure waves propagating downstream from the leading edge and upstream from the trailing edge. The difference goes to zero when the slower upstream wave passes off the leading edge. This difference is analogous to the impulsive, noncirculatory loads experienced in incompressible flow which are known to affect stability. Hence, the conclusion that only the generalized Φ_I solution is required to study stability is not supported.

Since solutions for this pressure difference are not available, the remainder of this paper is concerned with the application of generalized Φ_I solutions. It should be borne in mind that the missing portion of the solution is not treated by any current analysis technique, and its effect on stability boundaries is expected to be a small perturbation. Accordingly, the techniques presented in this paper should be compared to alternative techniques based upon traditional oscillatory aerodynamic theory.

Solution of the Aeroelastic Equations of Motion

In this section, generalized aerodynamic theory is used to calculate root loci and transient responses, and the use of augmented state techniques for calculating approximate solutions is summarized. The root loci determined by using the generalized Φ_I solution are termed exact root loci in accordance with common practice, although the preceding discussion indicates that a portion of the solution has been omitted.

Exact Solution

The Laplace transformed equations of motion of the section shown in Fig. 1 may be written as follows:

$$A(s)X(s) = Gu_c(s) \tag{4}$$

where

$$A(s) = [M_s s^2 + B_s s + K_s - Q_I(s)]$$

$$X^T(s) = [h(s)\ \alpha(s)\ \beta(s)\ \gamma(s)]$$

$$u_c^T = [\beta_c(s)\ \gamma_c(s)]$$

The matrix of aerodynamic load coefficients $Q_I(s)$ is given for incompressible flow by the equation

$$Q_I(s) = (1/\pi\mu)(U/b)^2\{M_{nc}\bar{s}^2 + B_{nc}\bar{s} + K_{nc} + C(\bar{s}) \times R[S_2\bar{s}+S_1]\} \tag{5}$$

Table 1 Parameters for three- and four-degree-of-freedom typical sections

	a) Three degrees of freedom, $M=0$	b) Three degrees of freedom, $M>1$	c) Four degrees of freedom, $M=0$
ω_α, rad/s	100	100	100
ω_h, rad/s	50	50	50
ω_γ, rad/s	300	317	500
ω_β, rad/s	...	...	500
μ	40	40	40
a	−0.4	0	−0.4
c	0.6	0.6	0.6
x_α	0.2	0.2	0.2
r_α^2	0.25	0.25	0.25
x_β, x_γ	0.0125	0.0125	0.0125
r_β^2, r_γ^2	0.00625	0.00625	0.00625
$\zeta_\beta, \zeta_\gamma$	0	0	0.1
b, m	...	1.35	...
a, m/s	...	333	...

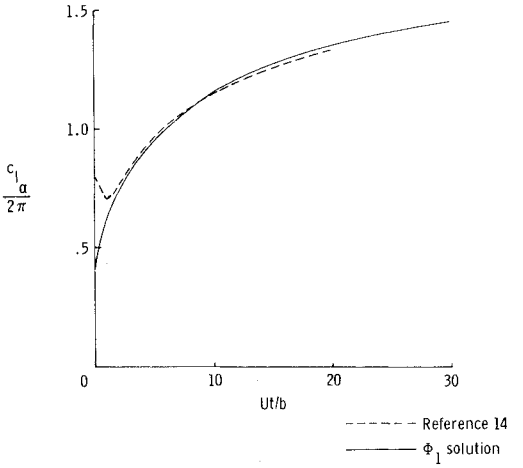

Fig. 2 Indicial lift due to impulsive plunging at Mach 0.8.

In supersonic flow,

$$Q_I(s) = \frac{8pb^2U^2\bar{s}^2}{\sqrt{M^2-1}}\{M_a(\bar{s})\bar{s}^2 + B_a(\bar{s})\bar{s} + K_a(\bar{s})\} \tag{6}$$

The generalized reduced frequency is $\bar{s}=sb/U$. The matrices in Eqs. (5) and (6) are given in Refs. 5 and 7.

In Eq. (5), the Theodorsen function $C(\bar{s})$ involves modified Bessel functions, whereas the matrices in Eq. (6) involve ordinary Bessel functions. The former functions are multiple-valued and have branch cuts along the negative real axis, while the latter functions are single-valued and have an infinite number of zeros.

Exact Root Loci of Aeroelastic Modes

Equation (4) is linear, and the stability of the airfoil section is determined by the zeros of the determinant of $A(s)$, the characteristic equation of the system. The loads defined by Eqs. (5) or (6) are valid for arbitrary values of the Laplace transform variable s. Since they contain nonrational functions of $\bar{s}$, e.g., $C(\bar{s})$, many of the commonly used eigenvalue routines cannot be used. Consequently, a computer program was developed to determine the roots of the characteristic equation by numerical iteration. A gradient search algorithm was employed in which the gradient was calculated by finite differences. The roots corresponding to the structural degrees of freedom were calculated, and root loci of three-degree-of-freedom sections with trailing-edge control surfaces are presented below.

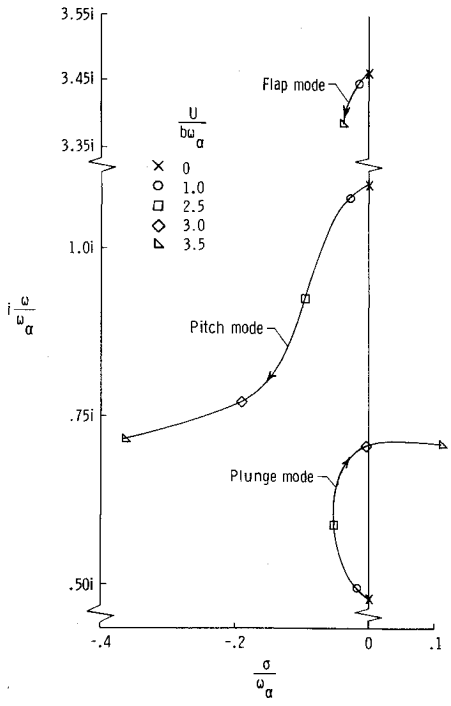

Fig. 3 Locus of roots of a three-degree-of-freedom section as a function of $U/b\omega_\alpha$ in incompressible flow.

Incompressible Two-Dimensional Flow

Table 1a lists the structural and geometric parameters for the three-degree-of-freedom section used in the following calculations. Fig. 3 shows the root locus of the section as a function of the nondimensionalized airspeed $U/b\omega_\alpha$. As the airspeed increases, the plunge and pitch modes approach each other in the stable left half-plane, with the plunge mode becoming the flutter mode at a value of $U/b\omega_\alpha$ of approximately 3.0.

Supersonic Two-Dimensional Flow

Table 1b lists the parameters for the three-degree-of-freedom section used to illustrate the aeroelastic root loci in supersonic flow. The loci of roots of this section are shown in Fig. 4 as a function of Mach number. At Mach 1.25, both the lowest-frequency coupled plunge-pitch mode and the flap mode are unstable. As the Mach number increases, both of these modes become stable at a Mach number of approximately 1.4. Above Mach 1.8, the remaining coupled plunge-pitch mode flutters.

Equation (4) also may be solved for $X(s)$, and transient responses may be calculated using the Laplace inversion integral. References 5 and 7 give examples of this process and show that the response is composed of portions termed "rational" and "nonrational." The examples indicate that the oscillatory motions characteristic of flutter are due entirely to the rational portion.

References 5 and 7 also compare root loci obtained from Eq. (4) with root loci obtained from approximate models that use augmented states to simulate unsteady aerodynamic effects. The resulting "Padé models"[15] are shown to give good approximations of the exact root loci in the vicinity of the $i\omega$ axis.

Finite-State Model of the Rational Portion of Aeroelastic Systems

The ability to calculate unsteady aerodynamic loads for arbitrary values of s, in combination with the insight acquired by the study of the Laplace inversion integral,[5,7] suggests a new technique of aeroelastic system modeling. This technique is summarized in this section. References 5 and 7 show that

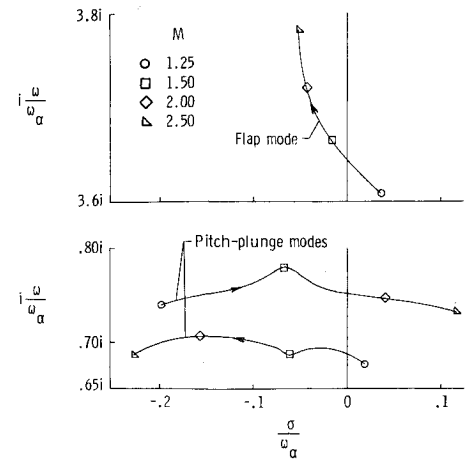

Fig. 4 Locus of roots of a three-degree-of-freedom section as a function of Mach number in supersonic flow.

two types of responses are possible for aeroelastic systems with nonrational transforms. The response of systems described by multiple-valued transforms contains rational and nonrational portions. The response of the nonrational portion is nonoscillatory and decays monotonically to zero. Systems described by single-valued nonrational transforms have an infinite set of simple poles. Usually, the poles due to the structural degrees of freedom are of primary interest. Models of either of these types of systems derived from the structural poles of the system are termed rational models. These models are desirable, since they describe the principal characteristics of the flutter problem.

The realization of the rational model in a finite-dimensional state space may be stated as the following theorem. *Theorem*: The linear system represented by

$$A(s)X(s)=G(s)u(s) \tag{7}$$

where $X(s)$ is n-dimensional, $u(s)$ is m-dimensional, and $A(s)$ and $G(s)$ may contain nonrational functions of s, may be approximated by the linear, constant-coefficient system

$$\dot{X}=FX+G_1u \tag{8}$$

where $X\epsilon E^N$, $u\epsilon E^m$, and $N=2n$. The system matrices may be given by $F=T\Lambda T^{-1}$, where

$$\Lambda=\text{diag}(s_1,s_2,\ldots,s_N), T_{\cdot i}=[A_i]_{\cdot 1}, G_1=\sum_{i=1}^{N}A_i$$

The s_i, $i=1,2,\ldots,N$ are the isolated singularities of $A(s)$, and the elements of the $N\times m$ residue matrices, A_i, are defined by $a^i_{jk}\tilde{}\ \text{res}^i_{jk}$.

The proof of the theorem is given in Ref. 5 and is based upon the unit rank of the A_i matrices. If $A(s)$ has only $2n$ poles, the rational model of Eq. (8) is an exact model of the rational portion of the system response. Reduced-order approximate models of the system may be constructed by deleting selected poles, since the algorithm usually can be applied for the case in which the dimension of X is $N<2n$.

The matrices F and G_1 describing the rational model of the three-degree-of-freedom section in Table 1a are given in Table 2a for $U/b\omega_\alpha=2.9$. The corresponding Padé model is given in Table 2b. The advantage of the rational model as opposed to the Padé model is that it does not require augmented states. A disadvantage of the model is a certain ambiguity regarding the relation of the states of the model to physical measurements of the system response. The deletion of the nonrational portion of the response results in the violation of the kinematic equations relating the states of the model as

Table 2 Rational and Padé models for a three-degree-of-freedom section [Mach 0, $U/b\omega_\alpha = 2.9$; F and G_I (s^{-1})]

a) Rational model

$$F = \left[\begin{array}{ccc|ccc} 0 & 0 & 0 & 1.0 & 0 & 0 \\ 0 & 0 & 0 & 0 & 1.0 & 0 \\ 0 & 0 & 0 & 0 & 0 & 1.0 \\ \hline -3395 & -1243 & -1139 & -10.04 & -0.1475 & 0.3564 \\ 3127 & -9758 & 6593 & 13.33 & -29.22 & -6.567 \\ -2858 & 29344 & -113723 & -27.78 & 44.98 & -5.120 \end{array}\right] \qquad G_I = \left[\begin{array}{c} 7.279 \\ -3.390 \\ 0.9792 \\ \hline -95.52 \\ -8648 \\ 115638 \end{array}\right]$$

b) Padé model

$$F = \left[\begin{array}{ccc|ccc|cc} 0 & 0 & 0 & 1.0 & 0 & 0 & 0 & 0 \\ 0 & 0 & 0 & 0 & 1.0 & 0 & 0 & 0 \\ 0 & 0 & 0 & 0 & 0 & 1.0 & 0 & 0 \\ \hline -2934 & -173.1 & -993.2 & -9.267 & -10.47 & -0.9598 & -10638 & -583.2 \\ 2514 & -11178 & 6399 & 12.30 & -15.52 & -4.820 & 14122 & 774.2 \\ -1579 & 32302 & -113319 & -25.61 & 16.50 & -8.755 & -29396 & -1611 \\ \hline 0 & 0 & 0 & 0 & 0 & 0 & 0 & 1.0 \\ 0 & 290 & 159.4 & 1.0 & 0.9 & 0.1487 & -1148 & -100.2 \end{array}\right] \qquad G_I = \left[\begin{array}{c} 0 \\ 0 \\ 0 \\ \hline 355.3 \\ -8939 \\ 115712 \\ \hline 0 \\ 0 \end{array}\right]$$

reflected by the nonzero value of the upper submatrix of G_I (Table 2a). The rational model might be expected to give better performance than the Padé model for points well removed from the $i\omega$ axis. The rational model is not restricted to the two-dimensional incompressible flow case. It is equally valid for compressible three-dimensional flow when used with truncated normal mode structural respresentations and aerodynamic loads calculated for arbitrary s. The usefulness of the rational model must be evaluated by its ability to predict the response of the system to feedback control.

Controllability and Observability of Aeroelastic Modes

The controllability and observability of the system

$$\dot{X} = FX + G_I u, \quad y = HX \tag{9}$$

was examined in Ref. 16, which shows that the system transfer function matrix may be written as

$$H(s) = \sum_{i=1}^{N} \frac{A_i}{s - s_i} \tag{10}$$

The matrix of residues, A_i, has a rank of one since it is the outer product of two vectors. The condition $A_i = 0$ occurs if either of these vectors is zero, and consequently the ith mode will be absent in the response. If $H = I$, there can be no observability problem, and uncontrollability is indicated by a pole-zero cancellation in all transfer functions.

These observations regarding pole-zero cancellations, controllability, and observability are the basis of the design technique used for the B-52 flutter mode control system[1] Control surface positions and sensor locations were chosen to achieve a large separation between the flutter mode and the nearest zero.

Controllability of a Two-Dimensional Typical Section

Since the aeroelastic mode shapes of flexible wings vary continuously as functions of Mach number and dynamic pressure, observability and controllability problems will occur at discrete values of these parameters, if they occur at all. The typical section is observable if measurements of h, α, β, and γ are assumed. Thus, the controllability of the section may be studied by examining the transfer functions of the Padé model.

Table 1c gives the parameters that define a nominal case for the four-degree-of-freedom section that was studied in incompressible flow. The leading- and trailing-edge control surfaces have spans of 20% of the chord and natural frequencies five times the torsion mode frequency. A small viscous damping is assumed to stabilize the flap modes.

Calculations were made with the Padé model for values of ω_h/ω_α equal to 0.25, 0.50, and 0.75. The system poles and zeros were determined at the flutter speed and at $\pm 25\%$ of this speed and are plotted in Fig. 5. It is evident that leading-edge flap control does not experience any controllability problems, since the locus of (h/γ) (s) and (α/γ) (s) tends to fall outside the range $\omega_h < \omega < \omega_\alpha$. The situation for the trailing-edge control is much different, with a near pole-zero cancellation occurring at the flutter speed for $\omega_h/\omega_\alpha = 0.5$. Thus, the case $\omega_h = 50$ rad/s is of interest as a worst-case design example, and studies of parameter variations for this configuration are of interest. The physical explanation for the uncontrollable mode is that, when the airfoil is oscillating in this uncontrollable mode, the structural and inertial forces and moments on the main section cancel the incremental lift and pitching moment due to flap motions.

Reference 5 studies the effect of the variation of the model parameters on the uncontrollability of the section. It is shown that varying the parameters associated with the main section (μ, x_α, r_α^2, and a) strongly influences controllability, whereas varying the parameters associated with the control surfaces has little effect.

Thus, for the purpose of active aeroelastic control, the leading-edge flap has advantages over the trailing-edge flap. However, the advantages are offset by the large destabilizing hinge moments that the leading-edge flap must carry, the power required to move the flap, and the violation of the

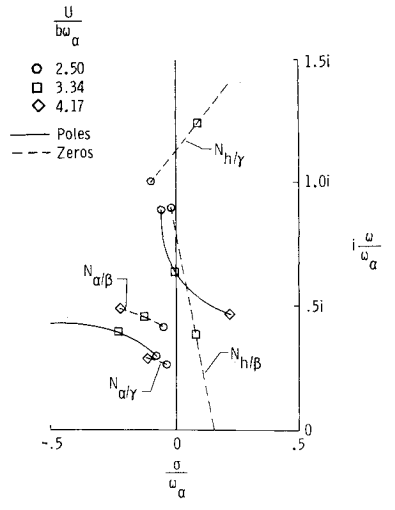

a) $\omega_h/\omega_\alpha = 0.25$

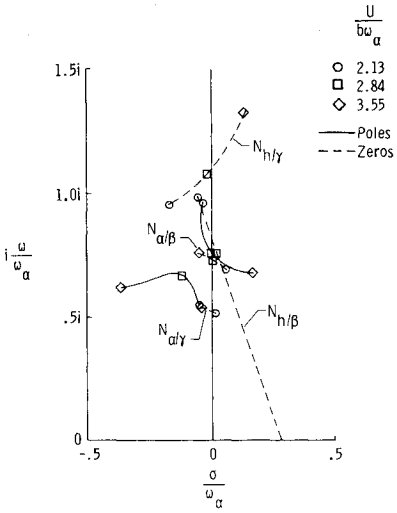

b) $\omega_h/\omega_\alpha = 0.50$

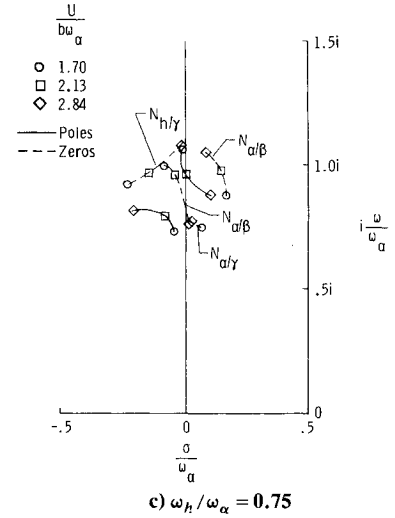

c) $\omega_h/\omega_\alpha = 0.75$

Fig. 5 Poles and zeros of a four-degree-of-freedom section vs $U/b\omega_\alpha$ and ω_h/ω_α in incompressible flow.

aerodynamic shape of the lifting surface in the critical leading-edge area. In addition, the proper design of a trailing-edge controller may permit the attainment of the active control objectives without encountering a controllability problem. The successful flight test of the B-52 flutter mode control system indicates that this is possible.[1]

It also should be noted that the desirability of leading-edge control is not as obvious for finite wings, which have a sequence of structural modes. Figure 5 shows that the leading-edge flap control does not encounter controllability problems because the zeros of the relevant transfer functions remain outside the range $\omega_h < \omega < \omega_\alpha$. This reasoning fails when it is applied to finite wings, however, since then the zeros may cause controllability problems with other modes.

Reference 5 also investigated the controllability of the section in subsonic and supersonic flow using the Padé model. The study showed that a similar uncontrollability condition occurred in subsonic flow. In supersonic flow, the section did not encounter a controllability problem with trailing-edge flap control.

Flutter Suppression Based on Aerodynamic Energy

The concept of controllability is useful in explaining the aerodynamic energy flutter suppression technique developed by Nissim.[4] This technique is based upon a consideration of the energy required to sustain simple harmonic oscillations of a two-degree-of-freedom typical section. If the sign of the energy is positive, indicating that energy must be supplied to the section to maintain the oscillation, the section is stable. Negative values of energy indicate that the airstream is supplying energy to the section, and it is assumed that the section would flutter if released. Nissim was able to derive a stability criterion that was independent of the structural and geometric parameters of the section. He argued that this formulation was desirable because of the wide variations in flight condition undergone by aircraft. He also concluded that flutter control using a single trailing-edge control surface was very difficult. Thus he developed a flutter control configuration that used both leading- and trailing-edge control surfaces. He determined the "optimized" feedback control law for the section shown in Fig. 1 in incompressible flow to be as follows:

$$\begin{bmatrix} \beta \\ \gamma \end{bmatrix} = \begin{bmatrix} -0.05 & -1.7 \\ 0.5 & 1.0 \end{bmatrix} \begin{bmatrix} h \\ \alpha \end{bmatrix} + \frac{1}{\omega_r} \begin{bmatrix} 0.45 & 0.2 \\ -0.5 & 1.0 \end{bmatrix} \begin{bmatrix} \dot{h} \\ \dot{\alpha} \end{bmatrix} \tag{11}$$

The Padé model may be used to study this control law. For the section parameters in Table 1c, the reference frequency ω_r is 76 rad/s. Figure 6 shows the locus of roots as a function of $U/b\omega_\alpha$ for the uncontrolled and controlled sections. The control law of Eq. (11) stabilizes the plunge and pitch modes for $0 < U/b\omega_\alpha < 3.9$, but the leading-edge flap mode is unstable throughout this range.

Nissim's technique was used to design a flutter suppression system[17] for a delta-wing wind-tunnel model that was tested at Mach 0.6, 0.7, 0.8, and 0.9. At the first three Mach numbers, the system could not be evaluated because of a severe leading-edge control surface instability. The instability was not encountered at Mach 0.9, and the flutter suppression system demonstrated a significant increase in the flutter dynamic pressure. It is suspected that the leading-edge surface instability is similar in nature to that analyzed in Fig. 6.

Thus, the aerodynamic energy design technique is deficient in that it neglects the control surface dynamics. In addition, because it attempts to define a flutter mode control system that is valid for all possible combinations of section parameters, the technique is incapable of producing a good design for a single trailing-edge control surface, since at least one combination of parameters can be found for which the section is uncontrollable (namely, the section described in Table 1c). This occurs even though the uncontrollability may occur for a combination of parameters outside the flight envelope of the wing.

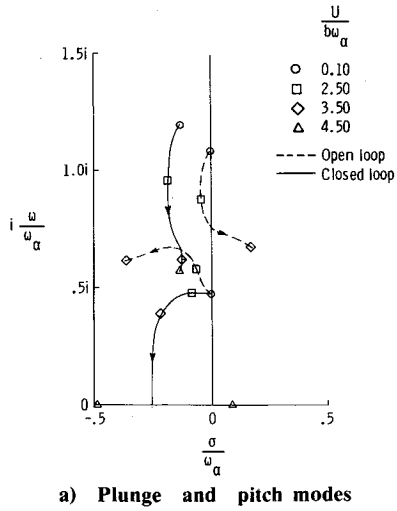

a) Plunge and pitch modes

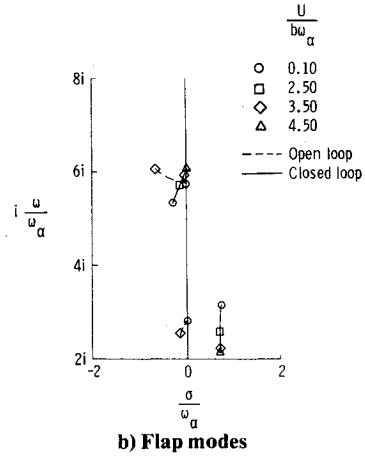

b) Flap modes

Fig. 6 Open- and closed-loop root loci of a four-degree-of-freedom section using the control law of Eq. (11).

Optimal Control of Aeroelastic Systems

In this section, active flutter control is studied by using the rational model. An appropriate performance index for the flutter problem is provided by the optimal regulator described in Ref. 18:

$$J=0.5\int_0^\infty [X^TAX+u^TBu]\,dt \tag{12}$$

Minimizing J while satisfying the differential equation constraint [Eq. (8)] is achieved by using the steady-state solution of the matrix Riccati equation. The resulting linear feedback control law is

$$u(t)=CX(t) \tag{13}$$

Reference 19 describes a digital computer program that is well suited to the solution of this problem and was utilized in the control law design of this section.

The problem of choosing the weighting matrices A and B remains. Although the underlying theory requires A to be positive semidefinite, computer algorithms that solve the regulator problem produce a stabilizing control law for $A=0$, that is, zero weighting on the state. This control law is particularly well suited to the flutter control problem in that its effect is to leave unchanged all stable eigenvalues, while open-loop unstable eigenvalues at $s=\sigma+i\omega$ are reflected about the $i\omega$ axis to $s=-\sigma+i\omega$. For structures with slightly supercritical flutter modes, this zero state weighting technique is attractive.

Reference 5 describes a modification of this design technique in which unstable eigenvalues are reflected about the line $\sigma=\nu$ instead of the $i\omega$ axis. This allows realistic flutter control at highly supercritical flutter conditions.

Table 3 Optimal regulator gains and eigenvalues for a three-degree-of-freedom section (Mach 0, $U/b\omega_\alpha=3.25$, $A=0$, $B=1$; poles in radians per second)

a) Rational model

$C=$ [2.901 −2.197 −0.09393 ¦ 0.04124 0.007558 0.0001064]

Mode	Open loop	Exact closed loop
Bending (flutter)	$6.420\pm71.03i$	$-4.975\pm69.94i$
Torsion	$-28.68\pm73.56i$	$-28.68\pm73.55i$
Flap	$-14.59\pm339.9i$	$-14.59\pm339.9i$

b) Padé model

$C=$ [2.517 −2.519 −0.1076 ¦ 0.0450 0.01168 0.0005183 ¦ −5.778 0.1436]

Mode	Open loop	Exact closed loop
Bending (flutter)	$6.987\pm71.01i$	$-5.790\pm71.48i$
Torsion	$-31.27\pm72.82i$	$-32.89\pm69.45i$
Flap	$-14.53\pm339.6i$	$-13.85\pm339.7i$
	−13.78	...
	−79.93	...

The optimal regulator solution was obtained for the three-degree-of-freedom section in Table 1a in incompressible flow at a value of $U/b\omega_\alpha$ of 3.25 by using the rational model and the Padé model. For this example, $c=0.5$. Table 3 gives the feedback gains and the open- and closed-loop eigenvalue locations for both the rational and the Padé models. The roots termed open loop are the eigenvalues of the appropriate uncontrolled F matrix. The roots termed exact closed loop were obtained by implementing the feedback control laws [Eq. (13)] in the exact system equations [Eq. (7)] and locating the exact closed-loop roots by iteration as described previously. This point is important, since it indicates how the rational model feedback gains are used. Although these gains are computed for the state of the rational model, they are used in the foregoing sense to multiply physical measurements of the system and thereby produce the feedback control command.

If the linear models represented by $\dot{X}=FX+G_Iu$ exactly described the dynamics of the section, the closed-loop roots would be identical to the open-loop roots except for a sign change in the real part of the unstable roots. Deviations of the roots away from this condition indicate the presence of unmodeled (nonrational) effects.

Table 3 shows that the feedback gains from corresponding states of the two models are comparable and that both stabilize the flutter mode. The distance of the closed-loop flutter pole from its anticipated location ($s=-6.42\pm71.03i$) is an indication of the ability of the models to deal with the unmodeled portion of the system. For the rational model, $|\Delta s|=1.56$ rad/s; for the Padé model, $|\Delta s|=1.29$ rad/s. It is interesting that these numbers are of comparable magnitude even though the Padé model attempts to simulate the nonrational effects of the aerodynamic loads with its augmented states. The corresponding distances for the other two modes illustrate a basic difference between the models. The rational model is an exact model of the rational portion of the system, and the regulator design leaves the exact stable poles of the rational model unchanged, whereas the Padé model design shifts the stable poles slightly.

Figure 7 shows the effect on the exact closed-loop plunge and pitch pole locations of off-design airspeeds, $U/b\omega_\alpha$, from 0.5 to 4.0. The gains in Table 3 were held constant throughout. The stable flap mode is not shown. Both closed-loop systems are unstable below the open-loop flutter speed of

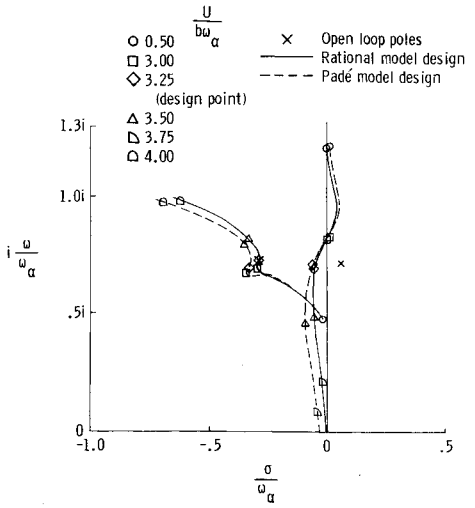

Fig. 7 Effect of off-nominal values of $U/b\omega_\alpha$ on the closed-loop plunge and pitch poles of a three-degree-of-freedom section in incompressible flow using the optimal regulator gains of Table 3.

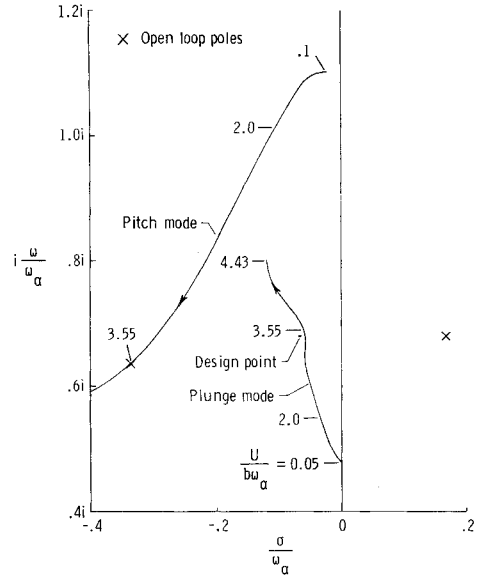

Fig. 8 Effect of off-nominal values of $U/b\omega_\alpha$ on the closed-loop poles of a four-degree-of-freedom section in incompressible flow.

3.0. This is due to the near uncontrollability of this section by the trailing-edge control surface at this airspeed. Hence this worst-case design is not practical. The identification of configurations with controllability problems is a requirement of any flutter control study. The solution of a controllability problem may be simply to relocate or resize a control surface. Multiple control surfaces may be considered, although this probably is not required.

The effect of two control surfaces was studied by using the four-degree-of-freedom section in Table 1c. Figure 5b illustrates the nature of the flutter mode that was studied at a value of $U/b\omega_\alpha$ of 3.55. The flutter mode is unstable, with a damping ratio of -0.23, and the airspeed is 25% above the flutter speed. In addition, this section is nearly uncontrollable by the trailing-edge control surface at a value of $U/b\omega_\alpha$ of 2.84. The rational model regulator design was obtained with the flutter mode reflected about the line where $\sigma = 5$ rad/s. Figure 8 shows the plunge and pitch modes for the resulting design. The open-loop poles are shown at the design airspeed, and the exact closed-loop poles are shown for $0.05 < U/b\omega_\alpha < 4.43$. The design point regulator feedback gains were held constant. The plunge and pitch modes, as well as the flap modes, are stable throughout this speed range,

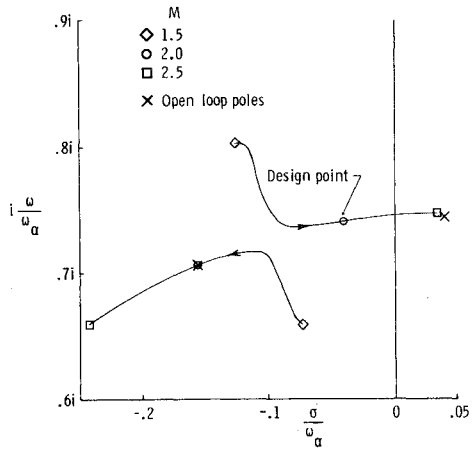

Fig. 9 Effect of off-nominal values of Mach number on the closed-loop plunge and pitch modes of a three-degree-of-freedom section in supersonic flow.

although a separate calculation shows that the airfoil is statically divergent at a $U/b\omega_\alpha$ of 3.98.

The optimal control of a three-degree-of-freedom section also was investigated in supersonic flow. The section of Table 1b was studied at Mach 2.0 by using the rational model. The weighting matrices were $A = 0$ and $B = 1$. Figure 9 shows the open-loop poles and the exact closed-loop poles for Mach numbers from 1.5 to 2.5. The distance between the design point and the exact closed-loop pole at the design Mach number indicates that the unmodeled nonrational effects are slight. The flap mode is stable throughout this Mach number range. One of the coupled plunge-pitch modes flutters at a Mach number of approximately 2.3, whereas the open-loop flutter boundary is approximately Mach 1.8.

These examples indicate the usefulness of the rational model for active flutter control. Although no augmented states are necessary, the use of optimal regulator techniques does require full state feedback. The preceding examples assumed the availability of measurements of the total physical state. The problem of state estimation in connection with rational model design techniques remains to be studied.

Concluding Remarks

This paper considers the application of generalized unsteady aerodynamic theory to the problem of the active control of elastic vehicles. Although certain details of transient aerodynamic effects are not modeled, extensive usage has verified the applicability of the oscillatory aerodynamic theory upon which the generalized theory is based. The theory allows the calculation of the exact root loci of aeroelastic modes and verifies the correctness of augmented state active flutter control techniques. With respect to typical sections in two-dimensional subsonic flow, it is shown that trailing-edge control surfaces may encounter a controllability problem for certain combinations of parameters. This identifies the reason for the failure of the aerodynamic energy flutter control technique in treating this case. The identification of rational and nonrational portions of the system response leads to the concept of the rational model. The rational model is a linear, finite-state, constant-coefficient model that describes the transient response typifying flutter phenomena. Active flutter control using the rational model and the optimal regulator design technique is studied in incompressible and supersonic flow. The examples presented show that the unmodeled nonrational effects have only small effects on the performance of the flutter control laws.

References

[1] Roger, K.L., Hodges, G.E., and Felt, L., "Active Flutter Suppression—A Flight Test Demonstration," *Journal of Aircraft*, Vol. 12, June 1975, pp. 551-556.

[2]Turner, M.R., "Active Flutter Suppression," *Flutter Suppression and Structural Load Alleviation,* AGARD-CP-175, July 1975, pp. 2-1 to 2-14.

[3]Dressler, W., "Control of an Elastic Aircraft Using Optimal Control Laws," *Impact of Active Control Technology on Airplane Design,* AGARD-CP-157, June 1975, pp. 9-1 to 9-11.

[4]Nissim, E., "Flutter Suppression Using Active Controls Based on the Concept of Aerodynamic Energy," NASA TN D-6199, 1971.

[5]Edwards, J.W., "Unsteady Aerodynamic Modeling and Active Aeroelastic Control," Stanford Univ., SUDAAR 504, Feb. 1977.

[6]Edwards, J.W., "Unsteady Aerodynamic Modeling for Arbitrary Motions," *AIAA Journal,* Vol. 15, April 1977, pp. 593-595.

[7]Edwards, J.W., Ashley, H., and Breakwell, J.V., "Unsteady Aerodynamic Modeling for Arbitary Motions," AIAA Paper 77-451, March 1977.

[8]Theodorsen, T., "General Theory of Aerodynamic Instability and the Mechanism of Flutter," NACA Rept. 496, 1934.

[9]Theodorsen, T. and Garrick, I.E., "Nonstationary Flow About a Wing-Aileron-Tab Combination Including Aerodynamic Balance," NACA Rept. 736, 1942.

[10]Theodorsen, T. and Garrick, I.E., "Mechanism of Flutter—A Theoretical and Experimental Investigation of the Flutter Problem," NACA Rept. 685, 1940.

[11]Jones, W.P., "Aerodynamic Forces on Wings in Non-Uniform Motion," British Aeronautical Research Council, R&M 2117, Aug. 1945.

[12]Van de Vooren, A.I., "Generalization of the Theodorsen Function to Stable Oscillations," *Journal of the Aeronautical Sciences,* March 1952, pp. 209-211.

[13]Bisplinghoff, R.L., Ashley, H., and Halfman, R.L., *Aeroelasticity,* Addison-Wesley, Reading, Mass., c. 1955.

[14]Lomax, H., Heaslet, M.A., Fuller, F.B., and Sluder, L., "Two- and Three-Dimensional Unsteady Lift Problems in High-Speed Flight," NACA Rept. 1077, 1952.

[15]Vepa, R., "On the Use of Pade Approximants To Represent Unsteady Aerodynamic Loads for Arbitrarily Small Motions of Wings," AIAA Paper 76-17, Jan. 1976.

[16]Gilbert, E.G., "Controllability and Observability in Multivariable Control Systems," *SIAM Journal on Control,* 1963, pp. 128-151.

[17]Sandford, M.C., Abel, I., and Gray, D.L., "Development and Demonstration of a Flutter-Suppression System Using Active Controls," NASA TR R-450, Dec. 1975.

[18]Bryson, A.E. Jr. and Ho, Y.-C., *Applied Optimal Control Revised: Optimization, Estimation, and Control,* Halsted Press, 1975.

[19]Hall, W.E. Jr. and Bryson, A.E. Jr., "Optimal Control and Filter Synthesis by Eigenvector Decomposition," Stanford Univ., SUDAAR 436, Nov. 1971.